Ramp initiation in a thrust wedge

John Panian & David Wiltschko

Department of Geology and Geophysics and Center for Tectonophysics, Texas A&M University, College Station, Texas 77843-3115, USA

Collisional mountain belts are characterized by fold and thrust belts that grow through sequential stacking of thrust sheets from the interior (hinterland) to the exterior (foreland) of the mountain belt[1–5]. Each of these sheets rides on a fault that cuts up through the stratigraphic section on inclined ramps that join a flat basal fault at depth. Although this stair-step or ramp–flat geometry is well known, there is no consensus on why a particular ramp forms where it does. Perturbations in fault shape[6,7], stratigraphy[8,9], fluid pressure[10,11], folding[2,12], and surface slope[13,14] have all been suggested as possible mechanisms. Here we show that such pre-existing inhomogeneities, though feasible causes, are not required. Our computer simulations show that a broad foreland-dipping plastic strain band forms at the surface near the topographic inflection produced by the previous ramp. This

strain band then migrates towards the rigid base, where the plastic strain is preferentially concentrated in a thrust ramp. Subsequent ramps develop toward the foreland in a similar fashion. Syntectonic erosion and deposition may strongly control the location of thrust ramps by enhancing or removing the surface point of initiation.

Restored cross-sections from diverse fold and thrust belts show that thrust ramp spacing is a function of thrust-sheet thickness[15–21] (Fig. 1). Specifically, ramp spacing decreases toward the foreland, in the same direction that the sedimentary package caught up in the thrusting thins. This observation suggests both that the mechanism for initiating thrust ramps is fundamental to the mechanics of fold and thrust belts and, while feasible and well-documented in some cases[22], local perturbations are not necessary to form thrust ramps.

We have conducted computer experiments to test whether ramp spacing can be explained without calling on local inhomogeneities. Our models use a modified Drucker–Prager constitutive relation that is a pressure-dependent, elastic–perfectly plastic rheology; see Methods. We incorporate an initial wedge-shape geometry that replicates the thinning of the sedimentary package toward the foreland[23–25]. The geometry of our finite-element model is 100 km in length and has a basal slope equal to the surface slope of 2°. The wedge lies upon a basal, rigid surface that represents basement rocks. The basal boundary condition is Coulomb frictional sliding. The rear wedge boundary is advanced in 10-m increments.

To characterize the initiation of a new thrust ramp, we begin at the point where the first backthrust–forethrust pair has formed at the rear of the wedge at 2,500 m of backstop displacement (Fig. 2a). It is not important how the first ramp forms. For example, we have run models where the basal friction abruptly changes. The point of change in friction is a ramp nucleation point. However, subsequent ramps form in the same manner as we show here. We have also run models with a basal perturbation in the form of a small step in the rigid base. In these models ramp development is essentially the same. In natural fold and thrust belts, the first ramp ultimately is the plate boundary.

After the initial ramp is formed (Fig. 2a), applying the next 10 m of displacement on the left boundary or backstop causes the structures to slide along the base. The basal displacement quickly tapers off to about 2 m displacement approximately 18 km from the origin and trends towards zero forelandwards with a subtle change in slope near 35 km (Fig. 2b). This first thrust sheet is moving up its ramp at ~35° (Fig. 2c).

The next ramp to form, in terms of plastic strain concentration, is initiated at the surface inflection of the previous existing ramp, and propagates in a broad band toward the base of the wedge. At 2,820 m of rear displacement, the band of plastic strain meets the base and begins to develop towards the foreland, initiating a new thrust ramp (Fig. 3a). The precursors for ramp initiation are: (1) increased basal displacement out to 35 km from the origin for this particular model (Fig. 3b) and (2) change in uplift path of the surface from nearly parallel to the thrust-sheet base to being inclined to it (Fig. 3c).

At 3,070 m of rearward displacement, a new thrust ramp is fully formed ~37 km from the origin (Fig. 4a). The forethrust clearly predominated over the backthrust in terms of plastic strain intensity. The basal displacement along the new thrust sheet has increased twofold (Fig. 4b) and the uplift path of the surface of the new thrust sheet approaches that of the first.

The pattern of displacement of the model surface illustrates the evolution of ramps. Figure 5a shows the difference in surficial displacement vectors between 2,500 and 2,820 m of backstop displacement. The onset of formation of the second ramp is clearly indicated 30 km from the backstop. Displacement vectors for material on the first ramp shallow. Simultaneously, the second ramp dominates abruptly as shown in the 2,820–3,070 m backstop displacement increment (Fig. 5b). The material on the first ramp has acquired a significant component of horizontal motion owing to displacement on the second ramp. This trend continues for subsequent ramps: motion on successive ramps adds a component

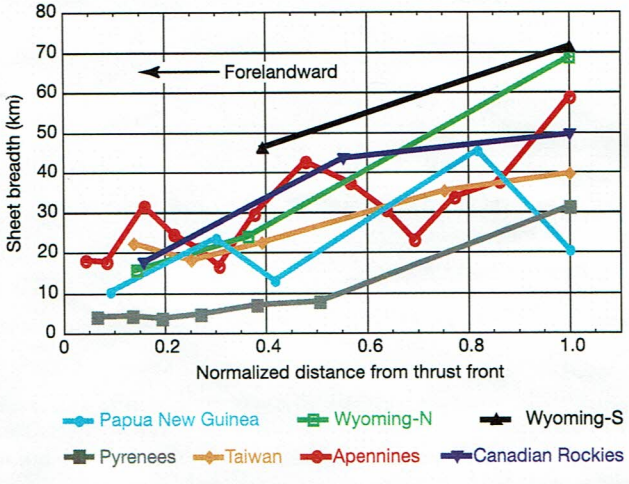

Figure 1 Thrust sheet breadth versus restored distance from the thrust front. The restored distance is measured to the most hinterlandward ramp and normalized to the total restored length of thrust sheets measured. Only thrust sheets having preserved hanging-wall cutoffs are included. Some grouping of minor splays was done. Sources were the Apennines[15]; northern Wyoming[16], Taiwan[17], southern Wyoming[18], the Canadian Rockies[19], Papua New Guinea[20] and the Pyrenees[21]. Owing to the incomplete nature of subsurface data, the variability in both the Apennine and Papua New Guinea cases could be decreased by slight reinterpretation of the seismic data. Nevertheless, as drawn, ramp spacing decreases toward the thrust front or foreland, in the same direction that the stratigraphic thickness decreases.

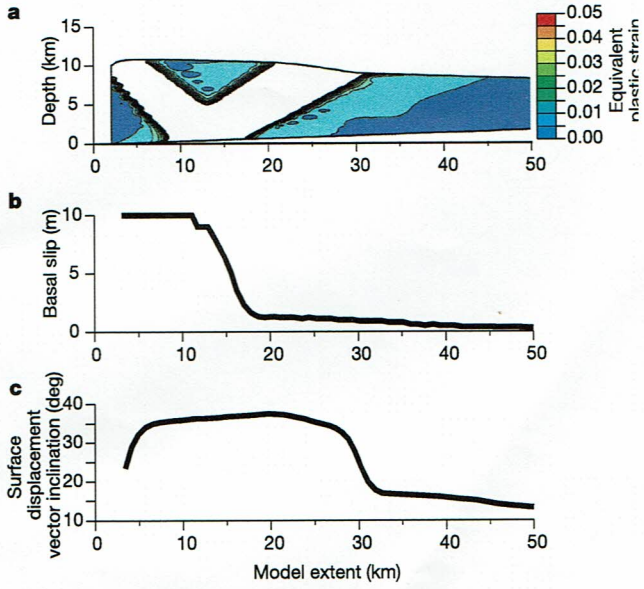

Figure 2 Thrust wedge after 2,500 m of backstop (left boundary) displacement. **a**, Equivalent plastic strains. A subtle increase in basal displacement in area **b** and the beginning of surface uplift. **b**, Basal displacement due to just the last 10-m increment of backstop displacement, that is, 2,490 to 2,500 m of backstop displacement. **c**, Inclination of displacement vectors on the surface of the model. The backthrust is subtly beginning, as indicated by the deflection in the 0.005 equivalent plastic strain contour at about 35 km in **a**, and in the same broad area in **c**. Compare Figs 3 and 4. Strains above 0.050 in **a** have been blocked out to emphasize deformation in the footwall. Although the model extends horizontally to 100 km, only the first 50 km are shown.

of horizontal motion to more interior ones and therefore their net motion relative to an external fixed reference frame appears to be shallower.

The pattern of surficial displacement vectors may indicate the location of a new thrust ramp prior to significant development and movement along that ramp. Geodetic measurements in active fold and thrust belts may be able to record this pattern. Inhomogeneities of the earthquake cycle may obscure the pattern for slowly moving faults.

The initiation of a thrust ramp is analogous to perturbation models for thrust duplex initiation[26,27]. Duplexes are found where ramps are constrained between quasi-parallel upper and lower thrust faults. The ramps link one with the other. In our wedge models there is no upper or roof thrust. Ramps initiate at the surface where an inflection has formed at the toe of a pre-existing ramp. Once this band reflects from the rigid base at the location of the basal or floor thrust, a conjugate, backthrust–forethrust set of plastic bands quickly localizes, with the forethrust band preferentially accumulating more plastic strain with backstop displacement. By analogy with duplexes, our perturbation would be the topographic inflection at the surface produced by a pre-existing thrust. This emphasizes the conclusion that perturbations are still required to form ramps. However, the perturbations we propose do not exist until the fold and thrust belt begin to develop. In this way our results are similar to those of ref. 12, which showed that thrust sheet spacing may be explained by folding. Specifically, the decrease in thrust spacing toward the foreland tracks wedge thinning because fold wavelength is strongly a function of layer thickness. Folds forming in front of the last ramp would localize thrust ramps at successively closer spacings toward the foreland.

Once a new thrust localizes, the previous ramp region behind the new thrust is displaced along the base with relatively little additional plastic straining. Most of the shortening that does take place behind the ramp causes uplift and shearing along the ramp. This surface displacement should appear in geodetically active fold and thrust belts as bulk horizontal translation with some uplift. Almost all plastic strain is located in the ramp (forethrust) regions and in their conjugate backthrusts. Immediately preceding localization of a new ramp, broad bands of plastic strain develop from the surface of the wedge towards the base. As the bands meet the base, they reflect upwards towards the surface of the wedge at an angle. The bands quickly, in terms of backstop displacement steps, become narrower, forming a backthrust–forethrust pair. With increasing displacement, the forethrust intensifies in plastic strain, while the backthrust lessens; successive thrust ramps form in a similar way within a thrust

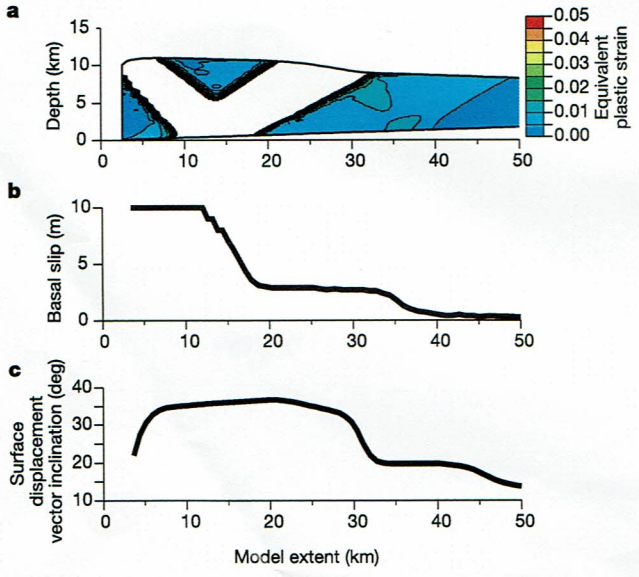

Figure 3 Thrust wedge deformation after 2,820 m of backstop displacement. **a**, Equivalent plastic strains. **b**, Basal displacement due to last 10-m increment of backstop displacement. **c**, Inclination of displacement vectors on the surface of the model. The conjugate shear band is now well developed, as can be seen in the 0.010 strain contour (**a**), increased basal slip behind the forming ramp (**b**) and an increase in inclination of surface displacement (**c**).

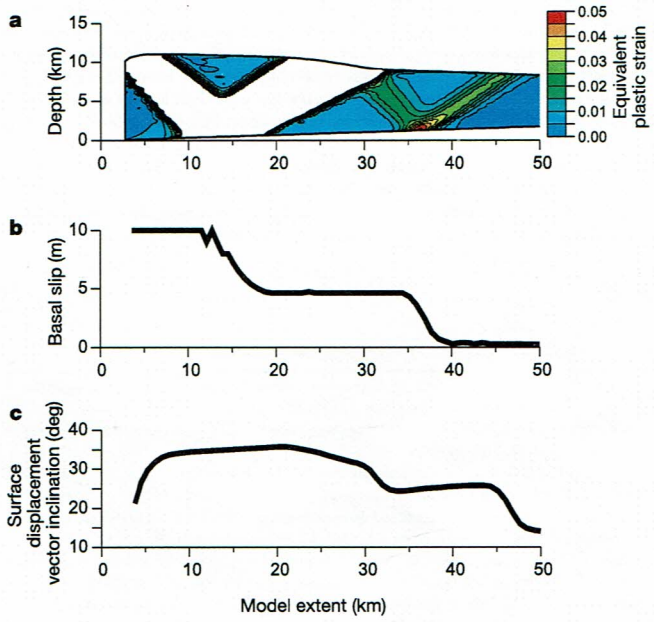

Figure 4 Thrust wedge deformation after 3,070 m of backstop displacement. **a**, Equivalent plastic strains. **b**, Basal displacement due to last 10-m increment of backstop displacement. **c**, Inclination of displacement vectors on the surface of the model. The forward ramp is now well developed with strains up to 0.050 at the base (**a**), basal slip nearly half that of the backstop (**b**) and an 30° inclination of surface displacement, that is, a typical ramp angle (**c**).

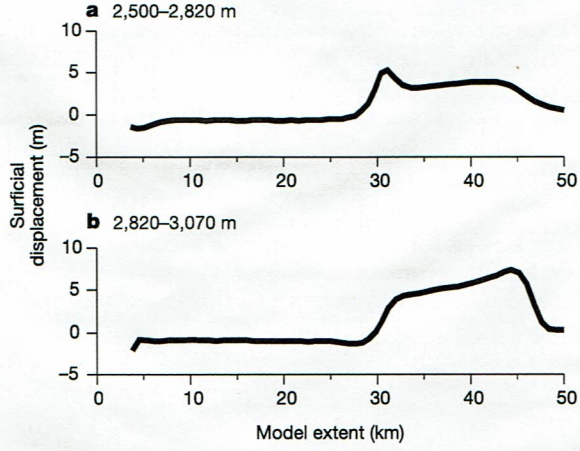

Figure 5 Magnitude of model surface displacement accumulated during two intervals of backstop displacement. **a**, Surface displacement magnitude accumulated from 2,500 to 2,820 m of backstop displacement. **b**, Surface displacement magnitude accumulated from 2,820 to 3,070 m of backstop displacement. Note the marked increase in surface displacement from ramp initiation (**a**) to the production of a well-developed ramp (**b**).

wedge. We propose that the strain intensification of each forethrust is a product of the build-up of the surface slope behind the forethrust and the tapered geometry of the wedge. □

Methods

We used the commercial finite-element software package, ABAQUS, to calculate the plastic strains and displacements in our models[28]. The yield function, F, is defined as:

$$F = aq^b - p - p_t \quad (1)$$

where p is the mean stress. q, the equivalent Mises stress, is defined as:

$$q = \sqrt{\frac{3}{2}\sigma'_{ij}\sigma'_{ji}} = \sqrt{3J_2} \quad (2)$$

J_2 is the second variant of deviatoric stress, where $\sigma'_{ij} = \sigma_{ij} - p\delta_{ij}$ is the deviatoric stress tensor. p_t represents the mean pressure tensile strength of the material. a and b in equation (1) are material parameters, independent of plastic deformation, that define the concavity of the yield surface in stress space. The three material parameters defined above (a, b, and p_t) are determined by a least-squares fit to triaxial test data. Data for our models were limited to those studies done on sedimentary rock under at least three different confining pressures no larger than about 250 MPa, or approximately 10 km depth. We used yield stress versus confining pressure values for a sandstone[29] that were about average for all the sedimentary rocks for which data exist. The material parameters in equation (1) are $a \approx b \approx 1$ and $p_t \approx 0$, which is identical for most of the yield stress data used in our models. The equivalent plastic strain measure[28,30] is defined as:

$$\bar{\varepsilon}^p = \int \sqrt{\frac{\sigma_{ij} d\varepsilon_{ij}^{pl}}{p}} \quad (3)$$

Received 10 June 2003; accepted 13 January 2004; doi:10.1038/nature02334.

1. Bally, A. W., Gordy, P. L. & Stewart, G. A. Structure, seismic data, and orogenic evolution of the southern Canadian Rocky Mountains. *Can. J. Petrol. Geol.* **14,** 337–381 (1966).
2. Dahlstrom, C. D. A. Structural geology in the eastern margin of the Canadian Rocky Mountains. *Bull. Can. Petrol. Geol.* **18,** 332–406 (1970).
3. Armstrong, F. C. & Oriel, S. S. Tectonic development of Idaho-Wyoming thrust belt. *Am. Assoc. Petrol. Geol. Bull.* **71,** 1847–1866 (1965).
4. Wiltschko, D. V. & Dorr, J. A. Timing and deformation in overthrust belts and foreland of Idaho, Wyoming, and Utah. *Am. Assoc. Petrol. Geol. Bull.* **67,** 1304–1322 (1993).
5. Jordan, T. E., Allmendinger, R. W., Damanti, J. F. & Drake, R. E. Chronology of motion in a complete thrust belt; the Precordillera, 30-31° S., Andes Mountains. *J. Geol.* **101,** 135–156 (1993).
6. Wiltschko, D. V. & Eastman, D. B. Role of basement warps and faults in localizing thrust-fault ramps. *Geol. Soc. Am. Mem.* **158,** 177–190 (1982).
7. Knipe, R. J. Footwall geometry and the rheology of thrust sheets. *J. Struct. Geol.* **7,** 1–10 (1985).
8. Bombalakis, E. G. Thrust–fault mechanics and origin of a frontal ramp. *J. Struct. Geol.* **8,** 281–290 (1986).
9. Platt, J. P. The mechanics of frontal imbrication, a first-order analysis. *Geologische Rundschau* **77,** 577–589 (1986).
10. Davis, D., Suppe, J. & Dahlen, F. A. Mechanics of fold-and-thrust belts and accretionary wedges. *J. Geophys. Res.* **88,** 1153–1172 (1983).
11. Cello, G. & Nurr, A. Emplacement of foreland thrust systems. *Tectonics* **7,** 261–272 (1988).
12. Goff. D. F., Wiltschko, D. V. & Fletcher, R. C. Decollement folding as a mechanism for thrust-ramp spacing. *J. Geophys. Res.* **101,** 11341–11352 (1996).
13. Panian, J. & Pilant, W. L. A possible explanation for foreland thrust propagation. *J. Geophys. Res.* **86,** 8607–8615 (1990).
14. Goff, D. F. & Wiltschko, D. V. Stresses beneath a ramping thrust sheet. *J. Struct. Geol.* **14,** 437–449 (1992).
15. Bally, A. W., Burbi, L., Cooper, C. & Ghelardoni, R. Balanced sections and seismic reflection profiles across the central Apennines. *Mem. Soc. Geol. It.* **35,** 257–310 (1986).
16. Royse, F. Jr, Warner, M. A. & Reese, D. L. *Deep Drilling Frontiers of the Central Rocky Mountains* 41–54 (Rocky Mountain, Assoc. Geol, 1975).
17. Suppe, J. A retrodeformable cross section of northern Taiwan. *Proc. Geol. Soc. China* **23,** 46–55 (1980).
18. Dixon, J. S. Regional structural synthesis, Wyoming salient of western overthrust belt. *Am. Assoc. Petrol. Geol. Bull.* **66,** 1560–1580 (1982).
19. Price, R. A. & Mountjoy, E. W. Geologic structure of the Canadian Rocky Mountains between Bow and Athabasca rivers—a progress report. Structure of the southern Canadian Cordillera. *Geol. Assoc. Can. Spec. Pap.* **6,** 7–25 (1970).
20. Hill, K. C. Structure of the Papuan fold belt, Papua New Guinea. *Am. Assoc. Petrol. Geol. Bull.* **75,** 857–872 (1991).
21. Williams, G. D. Thrust tectonics in the south central Pyrenees. *J. Struct. Geol.* **7,** 11–17 (1985).
22. Kraig, D. H., Wiltschko, D. V. & Spang, J. H. Interaction of basement uplift and thin skinned-thrusting, Moxa arch and the Western Overthrust Belt, Wyoming: A hypothesis. *Am. Assoc. Petrol. Geol. Bull.* **99,** 654–662 (1987).
23. Elliot, D. The motion of thrust sheets. *J. Geophys. Res.* **81,** 949–963 (1976).
24. Chapple, W. M. Mechanics of thin-skinned fold-and-thrust belts. *Geol. Soc. Am. Bull.* **89,** 1189–1198 (1978).
25. Makel, G. & Walters, J. Finite-element analysis of thrust tectonics: computer simulation of detachment phase and development of thrust faults. *Tectonophysics* **226,** 167–185 (1993).
26. Mandl, G. & Shippam, G. K. Mechanical model of thrust sheet gliding and imbrication. In *Thrust and Nappe Tectonics* 79–98 (Geol. Soc. Lond. Spec. Publ., 1981).
27. Davies, R. K. & Fletcher, R. C. Shear bands in a plastic layer at yield under combined shortening and shear: A model for the fault array in a duplex. In *Deformation Mechanisms, Rheology and Tectonics,* 123–131 (Geol. Soc. Lond. Spec. Publ. 54, 1990).
28. Hibbitt, H. D., Karlson, B. I. & Sorenson, E. P. *ABAQUS Theory Manual* (Hibbitt, Karlson & Sorenson, Pawtucket, RI, 1997).
29. Handin, J. & Hager, R. V. Experimental deformation of sedimentary rocks under confining pressure: Tests at room temperature on dry samples. *Am. Assoc. Petrol. Geol. Bull.* **41,** 1–50 (1957).
30. Malvern, L. E. *Introduction to the Mechanics of a Continuous Media* (Prentice-Hall, Englewood Cliffs, NJ, 1969).

Acknowledgements The NSF Tectonics programme supported this work. We wish to thank B. Johnson and J. Melosh for discussions.

Competing interests statement The authors declare that they have no competing financial interests.

Correspondence and requests for materials should be addressed to J.P. (jpanian@neo.tamu.edu).